Asymptotic dispersion for two-dimensional highly heterogeneous permeability fields under temporally fluctuating flow

Jean-Raynald de Dreuzy, Jesus Carrera, Marco Dentz, Tanguy Le Borgne

HAL Id: insu-00667637
https://insu.hal.science/insu-00667637

Asymptotic dispersion for two-dimensional highly heterogeneous permeability fields under temporally fluctuating flow

J.-R. de Dreuzy,[1,2] J. Carrera,[1] M. Dentz,[1] and T. Le Borgne[2]

[1] Temporal fluctuations of water flux have been investigated as a mechanism that strongly enhances transverse dispersion in heterogeneous media. Unfortunately, most results have been obtained by linear stochastic theories on permeability fields of limited variability. Worse, results are inconsistent regarding the impact of fluctuations on longitudinal dispersion, which motivates our work to find the effect of temporal velocity fluctuations on macrodispersion. We perform numerical Monte Carlo simulations for highly variable permeability fields of up to 800 correlation lengths. We find that fluctuations longitudinal to the main flow direction hardly modify macrodispersion because they do not alter the flow lines. Fluctuations transverse to the main flow direction not only increase transverse dispersion, which is well known, but also reduce the longitudinal macrodispersion in a significant and consistent way, which contradicts previous findings. The reduction of the longitudinal dispersion is comparable to the increase of transverse dispersion. Most surprisingly, for high heterogeneity, temporal fluctuations cause total (longitudinal plus transverse) macrodispersion to drop with respect to the steady state one. Enhancement of the transverse macrodispersion comes from both the increase of the transverse velocity variability and Lagrangian correlation. Reduction of the longitudinal macrodispersion results from the reduction of the Lagrangian correlation of the longitudinal velocity. That is, temporal fluctuations reduce longitudinal spreading both by breaking the fastest velocity paths on the plume front and by letting solute bypass the low-permeability zones that tend to block or trap the solute in steady state flow conditions.

1. Introduction

[2] Spreading and mixing of solutes control the extent of areas affected by point sources of pollution, the maximum concentrations and the rate of chemical reactions. Dispersion quantifies the rate of spreading. While mixing is different from spreading, both are intricately linked, so that large spreading rates usually lead to large mixing rates. It is not surprising that significant efforts have been devoted to characterizing dispersion [e.g., *Dagan*, 1989; *Gelhar et al.*, 1992; *Gelhar*, 1993; *Neuman et al.*, 1987]. Dispersion results from the spatial variability of water velocity, which in the context of permeable media is typically associated to the intrinsic heterogeneity of natural materials. However, one may expect dispersion to result also from temporal fluctuations of the velocity. Head gradients fluctuate in time at a range of scales: daily, as a result of evapotranspiration cycles or earth tides; yearly, as a result of seasonal variations in recharge, or hyperannually, as a result of dry and wet year sequences. On top of these, pumping causes an additional source of fluctuations.

[3] It is intuitive that temporal fluctuations of velocity should enhance dispersion. In fact, early researchers attributed large lateral spreading of carefully monitored plumes to unmodeled fluctuations in velocity direction [*Sudicky*, 1986; *Sykes et al.*, 1982]. Therefore, it is not surprising that many researchers have addressed the effect of temporal fluctuations on dispersion. What is surprising is how disparate are their findings. Prior to discussing these, we must point out that the problem is complex, that many assumptions are required to make it tractable, and that results are quite sensitive to these. Potential differences include how to define dispersion, how to represent it locally, and how to handle medium heterogeneities or velocity fluctuations.

[4] Regarding the definition of dispersion, the practical question from a modeling point of view is whether one can find an apparent dispersion coefficient that reproduces the observed plume, or breakthrough curve, without having to model explicitly the fluctuations. This is the approach adopted by earliest researchers [*Ackerer and Kinzelbach*, 1985; *Goode and Konikow*, 1990; *Kinzelbach and Ackerer*, 1986]. Instead, stochastic hydrologist tend to view dispersion as the rate of spreading of a solute plume (i.e., as the rate of growth of the second-order moments of the plume). One may evaluate the overall spreading rate of the ensemble of all possible solute plumes. This approach leads to the

[1]GHS, Institute of Environmental Analysis and Water Studies, CSIC, Barcelona, Spain.
[2]Géosciences Rennes, UMR CNRS 6118, Université de Rennes 1, Rennes, France.

concept of ensemble macrodispersion, which adds up the effects of uncertainty on plume location and actual spreading of each plume [*Dagan*, 1984; *Gelhar and Axness*, 1983; *Neuman et al.*, 1987]. Actual mean spreading is quantified by the effective dispersion [*Dentz et al.*, 2000; *Kitanidis*, 1988]. The effect of temporal fluctuations has been assessed on both ensemble macrodispersion [*Naff et al.*, 1989; *Rehfeldt and Gelhar*, 1992; *Zhang and Neuman*, 1996] and effective dispersion [*Cirpka and Attinger*, 2003; *Dentz and Carrera*, 2003, 2005]. Temporal fluctuations add another dimension of complexity to the stochastic definition of macrodispersion. Spatial (i.e., permeability realizations) and temporal (i.e., realizations of hydraulic gradient fluctuations) ensemble averaging are not interchangeable. Therefore, two additional macrodispersion coefficients can be defined by first averaging time fluctuations [*Dentz and Carrera*, 2003]. These additional definitions will be ignored here because of consistency with previous works and because they are not meaningful for assessing dispersion (every plume realization spreads under a single realization of temporal fluctuations). However, other choices may be more appropriate for other problems, such as delineation of protection zones [*Festger and Walter*, 2002].

[5] Differences in the treatment of temporal fluctuations also include differences in the representation of local mixing. These differences are largely motivated by the ultimate objective of the work. When the objective is to find an apparent dispersion coefficient to be included in a model, it is convenient to adopt local dispersion much larger in the longitudinal than in the transverse direction [*Ackerer and Kinzelbach*, 1985; *Goode and Konikow*, 1990; *Kinzelbach and Ackerer*, 1986]. When the objective is to assess the effect of spatial variability, then directionally dependent dispersion emerges from heterogeneity, so that local mixing can be represented by a constant scalar diffusion coefficient [e.g., *Dentz and Carrera*, 2003, 2005; *Dentz et al.*, 2011].

[6] The choice is not trivial. *Dentz and Carrera* [2003] and *Cirpka and Attinger* [2003] found that dispersion is enhanced by the coupling of spatial heterogeneity and temporal fluctuations. Therefore, temporal fluctuations of velocity in a homogeneous medium with constant dispersion would not result in enhanced spreading [*Dentz and Carrera*, 2003]. Instead, they would cause the whole plume to be displaced back and forth around its mean position, while spreading would continue unaffected by temporal fluctuations. In contrast, *Kinzelbach and Ackerer* [1986] found that the apparent transverse dispersivity increases in response to fluctuations. Actually, they found that the sum of apparent longitudinal and transverse dispersivities remains equal to the sum of the local dispersivities if only the orientation, but not the modulus, of mean velocity fluctuates in time. *Goode and Konikow* [1990] corrected this finding to mean the sum of dispersion coefficients. The point, however, remains that if the medium is homogeneous there is little, if any, growth of total (i.e., sum of longitudinal and transverse) dispersion.

[7] A significant source of complexity lies in the fact that velocity may fluctuate around its mean in the longitudinal and/or in the transverse directions. Moreover, it may fluctuate in absolute value and/or direction. These fluctuations may impact longitudinal and/or transverse dispersion coefficients. All researchers have found that transverse fluctuations of velocity (or fluctuations in direction) cause a significant increase in transverse dispersion. However,

while *Kinzelbach and Ackerer* [1986] and *Goode and Konikow* [1990] found the enhancement to be very large, stochastic researchers found that it is not so important [*Cirpka and Attinger*, 2003; *Dagan et al.*, 1996; *Zhang and Neuman*, 1996]. Results for all other combinations are much more disparate.

[8] The effects of velocity fluctuations on longitudinal dispersion are generally found to be much smaller than on transverse dispersion. However, while some find that longitudinal dispersion decreases with fluctuations in the direction [*Zhang and Neuman*, 1996], others find that it may decrease or increase [*Goode and Konikow*, 1990; *Rehfeldt and Gelhar*, 1992], increase [*Dentz and Carrera*, 2005] or remain unchanged [*Cirpka and Attinger*, 2003]. Similarly, fluctuations in the magnitude of velocity have been reported to either increase or decrease longitudinal dispersion [*Zhang and Neuman*, 1996] or to increase it [*Dentz and Carrera*, 2003]. It is clear that so disparate set of results demands a careful reanalysis.

[9] The objective of our work is to reanalyze the effect of velocity fluctuations on macrodispersion. This work is partly motivated by high heterogeneity and by the disparity of previous results, which are mostly analytical. Therefore, we need to perform highly accurate Monte Carlo simulations of conservative transport. The methodology adopted for these simulations is presented in section 2. Once validated against simple cases, simulation results are reported in section 3 for different degrees of spatial heterogeneity and temporal variability. For low heterogeneity and fluctuations, they are compared to analytical approximations. For higher degrees of heterogeneity and fluctuations, they are discussed qualitatively and by means of the Lagrangian velocity variability and correlations in section 4.

2. Model and Numerical Methods

[10] This study relies on classical model and numerical methods. We first summarize their assumptions and parameters. We second validate our numerical methodology.

2.1. Model

[11] The permeability field $K(\boldsymbol{x})$ is modeled by a 2-D lognormal field with a Gaussian isotropic correlation function such as

$$\langle Y'(\mathbf{x})Y'(\mathbf{x}')\rangle = \sigma_Y^2 \exp\left[-\left(\frac{|\mathbf{x}-\mathbf{x}'|}{\lambda}\right)^2\right], \qquad (1)$$

where $Y'(\mathbf{x}) = Y(\mathbf{x}) - \langle Y \rangle$ and $Y(\mathbf{x}) = \ln(K(\mathbf{x}))$, $\langle \; \rangle$ stands for spatial (ensemble) average σ_Y^2 is the lognormal permeability variance and λ is the isotropic correlation length. The computational domain is a rectangle of dimensions L_1 and L_2 in the two spatial dimensions x_1 and x_2 counted in terms of correlation length (L_1/λ, L_2/λ). Simulated conductivities are periodic on the $x_2 = 0$ and $x_2 = L_2$ boundaries (that is, $Y(x_1, 0) = Y(x_1, L_2)$) to facilitate imposing periodic boundary conditions, which will be required later.

[12] Temporal fluctuations in velocity are assumed to result from fluctuations of the boundary conditions, which induce a temporally varying spatial mean hydraulic gradient $\mathbf{J}(t) = \nabla h(\bar{x}, t)$. These fluctuations are modeled by an approximate method described subsequently. Without loss

of generality, we take the temporal mean hydraulic gradient $\bar{\mathbf{J}}$ aligned with the first direction $\bar{J}_i = \delta_{i1} J$ (the overbar stands for time averaging). Fluctuations are defined with respect to the temporal mean gradient in dimensionless form $\mathbf{v}(t) = \left(\mathbf{J}(t) - \bar{\mathbf{J}} \right)/J$ as a random process characterized by the two variances σ_{v1}^2 and σ_{v2}^2 of the fluctuations ν_1 and ν_2, respectively, parallel and orthogonal to the main flow direction, by the correlation coefficient ρ between those fluctuations, and by a Gaussian correlation function having the same correlation time τ in both directions:

$$\overline{\mathbf{v}(t)\mathbf{v}^t(t')} = \begin{bmatrix} \sigma_{v1}^2 & \rho \cdot \sigma_{v1} \cdot \sigma_{v2} \\ \rho \cdot \sigma_{v2} \cdot \sigma_{v1} & \sigma_{v2}^2 \end{bmatrix} \exp\left[-\left(\frac{|t - t'|}{\tau} \right)^2 \right]. \tag{2}$$

[13] This model of fluctuations generalizes the one of *Dentz and Carrera* [2005] by introducing the correlation between the longitudinal and transverse fluctuations and by allowing σ_{v1}^2 to be different from σ_{v2}^2.

[14] The time-dependent velocity $\mathbf{u}(x,t)$ is derived by using a quasi steady state approximation equivalent to neglecting storativity. Temporal fluctuations of the boundary conditions are assumed to transfer instantaneously everywhere in the field, which is a good approximation for confined moderately small aquifers. This simplification facilitates the interpretation of results, by eliminating one independent variable, and its solution, by taking advantage of linearity to get the time-dependent velocity fields from the superposition of two velocity fields $\mathbf{u}_1$ and $\mathbf{u}_2$.

[15] Here, $\mathbf{u}_1$ is obtained from the classical steady state diffusion equation with fixed heads on the $x_1 = 0$ and $x_1 = L_1$ boundary and with periodic flux boundary conditions on the $x_2 = 0$ and $x_2 = L_2$ boundaries (Figure 1):

$$\begin{aligned} & \nabla[K(\mathbf{x})\nabla h_1(\mathbf{x})] = 0 \\ & h_1|_{x_1=0} = 0 \\ & h_1|_{x_1=L_1} = L_1 \, |\bar{\mathbf{J}}| \\ & \mathbf{u}_1|_{x_2=0} \cdot \mathbf{n}|_{x_2=0} = -\mathbf{u}_1|_{x_2=L_2} \cdot \mathbf{n}|_{x_2=L_2}, \end{aligned} \tag{3}$$

where velocity $\mathbf{u}_1$ is obtained from the head gradient by Darcy's law: $\mathbf{u}_1(\mathbf{x}) = -K(\mathbf{x})\nabla h_1(\mathbf{x})/\theta$. The fixed boundary heads are chosen to produce a macroscopic $\bar{\mathbf{J}}$ head gradient. $\mathbf{u}_2$ is obtained by rotating these boundary conditions by 90°:

$$\begin{aligned} & \nabla[K(\mathbf{x})\nabla h_2(\mathbf{x})] = 0 \\ & h_2|_{x_2=0} = 0 \\ & h_2|_{x_2=L_2} = L_2 \, |\bar{\mathbf{J}}| \\ & \mathbf{u}_2|_{x_1=0} \cdot \mathbf{n}|_{x_1=0} = -\mathbf{u}_2|_{x_1=L_1} \cdot \mathbf{n}|_{x_1=L_1}. \end{aligned} \tag{4}$$

[16] At each time, the velocity $\mathbf{u}(x_1,x_2,t)$ is obtained as a simple linear combination of $\mathbf{u}_1$ and $\mathbf{u}_2$:

$$\mathbf{u}(\mathbf{x},t) = [1 + \nu_1(t)] \cdot \mathbf{u}_1(\mathbf{x}) + \nu_2(t) \cdot \mathbf{u}_2(\mathbf{x}), \tag{5}$$

where ν_1 and ν_2 are the previously defined temporal fluctuations parallel and orthogonal to the main flow direction.

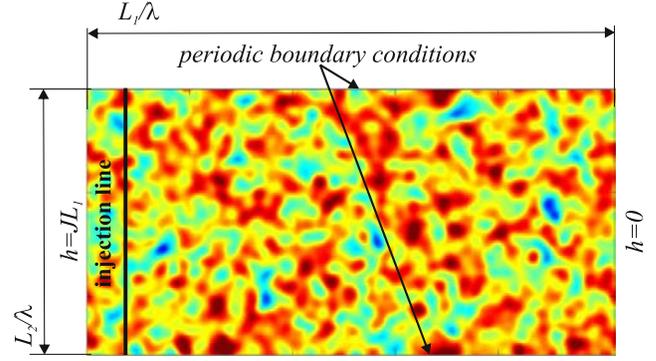**Figure 1.** Illustration of the numerical setting used to obtain $\mathbf{u}_1(\mathbf{x})$ on a small permeability field of size 50λ by 25λ. The typical sizes simulated in this study are 4 to 16 times larger. Periodic boundary conditions are applied both on the permeability field, on the flow and on the transport equations. These boundary conditions are rotated by 90° to obtain $\mathbf{u}_2(\mathbf{x})$. Under the pseudo steady state assumption, $\mathbf{u}_1$ and $\mathbf{u}_2$ are combined according to equation (5) to produce the temporally fluctuating velocity field $\mathbf{u}(\mathbf{x},t)$.

Note that $\mathbf{u}_1(\mathbf{x})$ and $\mathbf{u}_2(\mathbf{x})$ are vector fields having components in both spatial directions even though they are obtained by applying head gradients in a single direction. With this choice of boundary conditions, the spatial and temporal averaged velocity $\overline{\langle \mathbf{u}(\mathbf{x},t) \rangle}$ is equal to the geometrical average of the local permeabilities K_g times the mean hydraulic gradient $\bar{\mathbf{J}}$ divided by the porosity θ [*Matheron*, 1967]:

$$\overline{\langle \mathbf{u} \rangle} = -K_g \cdot \bar{\mathbf{J}}/\theta. \tag{6}$$

[17] Porosity is taken here as constant.

[18] The periodic boundary conditions imposed both on the permeability generation and on the flow equation orthogonally to the main flow direction ensures that the velocity statistics are not biased by the side of the domain, in contrast to the no-flow boundary conditions case [*Englert et al.*, 2006; *Salandin and Fiorotto*, 1998].

[19] Solutes are transported by advection and diffusion. Accepting that pore-scale dispersion may be directionally dependent, this work is restricted to the case of homogeneous local diffusion (as opposed to local velocity-dependent dispersion), on the assumption that tensorial dispersion will emerge in response to heterogeneity in hydraulic conductivity, because of simplicity and because it may be assumed that the choice will bear little effect on macrodispersion. Therefore, concentration c follows locally the classical advection diffusion equation:

$$\frac{\partial c}{\partial t} + \nabla \cdot (\mathbf{u}c) - \nabla \cdot (d \cdot \nabla c) = 0, \tag{7}$$

where d is the diffusion coefficient, which we take as constant. Periodic boundary conditions are also imposed for concentrations on the $x_2 = 0$ and $x_2 = L_2$ boundaries. That is, particles leaving the domain at $x_2 = 0$ are reintroduced at $x_2 = L_2$, and vice versa, but are labeled as having crossed the boundary. As a result, everything happens as if the

domain were replicated in the transverse directions. The plume can thus spread laterally outside of the physical limits of the domain.

[20] The ratio of advection to diffusion is classically described by the Peclet number Pe with

$$Pe = (\lambda \bar{u})/d. \tag{8}$$

[21] Injection is instantaneous on the full width of the domain L_2 orthogonally to the main flow direction. Injection is located downstream from the domain inlet by a distance of 10λ from the domain inlet to avoid boundary effects. Injection is proportional to flow. The large injection window is designed to speed up convergence to the asymptotic regime [Dentz et al., 2000], at least in the longitudinal direction.

2.2. Simulation Method

[22] The methodology is analogous to that used for deriving the 2-D asymptotic dispersion coefficients in steady state flows in presence of local diffusion or local hydrodynamic dispersion [Beaudoin et al., 2007, 2010; de Dreuzy et al., 2007]. To sample the stochastically defined permeability and temporal fluctuations model, we have chosen a basic Monte Carlo method.

[23] We use a fully parallelized simulation method to generate permeability fields and temporal fluctuations, and solve the flow and transport equations. The Fourier transform method, which ensures periodicity of the simulated field, is used through the parallel library fftw to generate the Gaussian correlated permeability fields [Frigo and Johnson, 2005; Gutjahr, 1989; Pardo-Iguzquiza and Chica-Olmo, 1993]. The computational domain is discretized in square grid cells ($dx_1 = dx_2 = l_m$). The size of the system in terms of correlation lengths (L_1/λ, L_2/λ) and the discretization of a correlation length in cells (λ/l_m) should be both large to ensure that asymptotic dispersion values are reached. We take for λ/l_m a classical value of 10 [Ababou et al., 1989; de Dreuzy et al., 2007]. Without time fluctuations, convergence is practically reached for values of L_1 ranging from 200 to 800 for $\sigma_Y = 1$ and $\sigma_Y = 3$, respectively [de Dreuzy et al., 2007]. To speed up convergence to the asymptotic regime, we choose a large injection window of 200 correlation lengths orthogonal to the main flow direction. These choices lead to a number of cells of the order of 10^8, justifying the need for parallel computing.

[24] We use a finite volume scheme with harmonic intermesh permeabilities to solve the flow equation [Chavent and Roberts, 1991] and the algebraic multigrid method of HYPRE to solve the yielded linear system [Erhel et al., 2009; Falgout et al., 2005]. Velocity is linearly interpolated in both directions from the cell faces [Pollock, 1988].

[25] A Monte Carlo realization is characterized by a realization of the conductivity field and a realization of the temporal fluctuations. This means that both conductivity field and temporal fluctuations change from realization to realization. The temporal fluctuation sequences are generated by a Cholesky decomposition from two independent Gaussian autocorrelated sequences μ_1 and μ_2 [Alabert, 1987; Davis, 1987; Le Ravalec et al., 2000]:

$$\begin{aligned} \nu_1(t) &= \sqrt{1 - \rho^2} \sigma_{\nu_1} \mu_1 + \rho \sigma_{\nu_1} \mu_2 \\ \nu_2(t) &= \sigma_{\nu_2} \mu_2. \end{aligned} \tag{9}$$

[26] Here, μ_1 and μ_2 have been generated with the same methods used for generating the permeability field. The only difference is that μ sequences are 1-D whereas permeability fields are 2-D. The discretization step of these sequences was set to one 10th of the correlation time to match what was chosen for the spatial discretization.

[27] We use random walk to simulate solute transport [Kinzelbach, 1988; Ramirez et al., 2008]. Particles are advected and diffused within the medium following the Fokker-Planck equation [Delay et al., 2005; Salamon et al., 2006; van Kampen, 1981]. Advection is simulated by a first-order explicit scheme. Between t and $t + dt$, a particle moves from positions $\mathbf{x}(t)$ to $\mathbf{x}(t + dt)$ by advection and diffusion:

$$\mathbf{x}(t + dt) = \mathbf{x}(t) + \mathbf{u}[\mathbf{x}(t), t]dt + \sqrt{2\,d\,dt}\, Z\, \mathbf{r} \tag{10}$$

with $\mathbf{u}[\mathbf{x}(t)]$ the velocity at position $\mathbf{x}$, Z a normalized Gaussian distributed random number and $\mathbf{r}$ a vector with uniform distribution of orientations. The time step evolves along the particle path according to the velocity magnitude of the crossed cells, much in the spirit of Wen and Gomez-Hernandez [1996]. More precisely, the time step is either proportional to the local advection time, which equals the cell size l_m divided by the maximum of the velocities computed on the cell borders noted $v_{x1+}, v_{x1-}, v_{x2+}, v_{x2-}$, in the x_1 and x_2 directions or to the diffusion time necessary to cross the cell:

$$dt = \frac{1}{\alpha} \min\left[\frac{l_m}{\max(v_{x1+}, v_{x1-}, v_{x2+}, v_{x2-})}, \frac{l_m^2}{2d} \right], \tag{11}$$

where α is an integer that approximates the number of time steps performed by the particle in the cell. In the simulations α is set to 20, meaning that a particle takes of the order of 20 steps to cross a cell.

2.3. Estimate of Effective Dispersion

[28] We estimate the asymptotic dispersion coefficient as the limit of the effective dispersion for large time. At large times, the effective and ensemble dispersion coefficients are equal [Dentz et al., 2000; Kitanidis, 1988]. Spreading of the solute in a single medium and temporal fluctuations realization is defined by the second centered moments

$$\sigma_k^{i2}(t) = \frac{1}{N_p} \sum_{j=1}^{N_p} x_k^{j,i}(t)^2 - \left(\frac{1}{N_p} \sum_{j=1}^{N_p} x_k^{j,i}(t) \right)^2, \tag{12}$$

where $x_k^{j,i}(t)$ denotes the position of the jth particle in the ith realization with $k = 1,2$ and N_p is the number of particles injected in a single realization. The growth rate of the second center moments in a single realization (of $Y(x)$ and $\mathbf{J}(t)$) is measured by the dimensionless longitudinal and transverse dispersion coefficients:

$$D_k^i(t) = \frac{1}{2\lambda \bar{u}} \frac{d\sigma_k^{i2}(t)}{dt}. \tag{13}$$

[29] Dispersion coefficients are normalized by $\lambda \bar{u}$. The effective second centered moment and dispersion coefficients

are defined as ensemble averages over N_R Monte Carlo realizations:

$$\sigma_k^2(t) = \frac{1}{N_R}\sum_{i=1}^{N_R}\sigma_k^{i2}(t) \tag{14}$$

$$D_k(t) = \frac{1}{N_R}\sum_{i=1}^{N_R}D_k^i(t). \tag{15}$$

[30] All time-dependent dispersion results will be presented against the dimensionless t_N defined as the time t normalized by the characteristic time necessary to cross a correlation length $\lambda/\bar{u}$ ($t_N = t\bar{u}/\lambda$).

[31] The asymptotic regime is observed over at least the last quarter of the simulation time range, i.e., over the time interval $\lfloor 0.75t_b^i, t_b^i\rfloor$ where t_b^i is the first breakthrough time of the ith realization, i.e., the time at which the first particle leaves the system by the $x_1 = L_1$ side. In this time range, dispersion does not display any systematic increasing or decreasing tendency. We thus define the realization-based asymptotic dispersion coefficient or macrodispersion coefficient as

$$D_{kA}^i = \frac{\int_{0.75t_b^i}^{t_b^i} D_k^i(t)dt}{0.25\,t_b^i}. \tag{16}$$

[32] The asymptotic dispersion coefficient is simply obtained by averaging over the number of simulations N_S:

$$D_{kA} = \frac{1}{N_S}\sum_{N_S}D_{kA}^i. \tag{17}$$

[33] The advantage to derive the asymptotic dispersion coefficient first on a realization basis is to adapt the averaging time range $\lfloor 0.75t_b^i, t_b^i\rfloor$ to the realization first breakthrough time rather than taking the minimum of the realization first breakthrough times t_b for all simulations.

2.4. Parameter Values

[34] The characteristic length is the correlation length λ and the characteristic time is the average time needed to cross one correlation length $\lambda/\bar{u}$. All dimensional parameters of the model can be expressed with respect to these two characteristic measures. Expressed in dimensionless form, the independent parameters of the model are the Peclet number (equation (6)) expressing the rate of advection to diffusion, the standard deviation of the permeability field distribution σ_Y, the standard deviation of the temporal fluctuations along and perpendicular to the mean flow gradient σ_{v1} and σ_{v2}, their correlation coefficient ρ and temporal fluctuation correlation time τ. The dimensionless value of the latter (normalized by the advection correlation time $\lambda/\bar{u}$) is also called the Kubo number:

$$\kappa = \frac{\tau\bar{u}}{\lambda}. \tag{18}$$

[35] As we are interested on the effects of spatial and temporal variabilities, we have fixed the Peclet and Kubo numbers while varying the three variances σ_Y, σ_{v1} and σ_{v2} and the correlation coefficient ρ. The Peclet number was set to 10^3 meaning a moderate diffusion compared to the average advection. The Kubo number was set to 1 because this value leads to significant effects of temporal fluctuations [*Dentz and Carrera*, 2005], and still makes it numerically feasible to simulate transport over many correlation times. The correlation coefficient ρ has been fixed either at 0 or at an intermediate value of 0.5. For heterogeneity, we have tested low, moderate and high-heterogeneity cases corresponding to values of σ_Y equal to 0.5, 1 and 3. For temporal fluctuations, we have also chosen low, intermediate and high fluctuations corresponding to σ_{v1} and σ_{v2} equal to 0.25, 0.5, and 1, respectively.

[36] Concerning the values of the numerical parameters, we have checked the convergence of the effective dispersion with the temporal discretization of the fluctuations, with the number of simulations and with the number of particles. The variability of the effective dispersion around an average value taken as its asymptotic values comes from the number of realizations more than from the number of particles per simulation. To estimate the decrease in variability, we use the standard deviation of the transverse effective dispersion during the fourth temporal quarter of the effective dispersion signal as a measure. For the largest effective dispersion variability corresponding to $\sigma_Y = 3$ and $\sigma_{v1} = \sigma_{v2} = 1$, the standard deviation of the D_{1A}^i's drops from 2.1 to 1.1 between 25 and 100 simulations. The latter implies a standard deviation around 0.01 for our estimate of D_{1A}. Following these convergence results and constrained by the available computation time, the results presented in this article have been obtained for a number N_S of simulations equal to 100 and 10^4 particles per simulation.

2.5. Verification

[37] We verify our methodology in two ways. First, without fluctuations, the computation of the asymptotic dispersion coefficient has been checked against the analytical approximation for low- and moderate-permeability heterogeneity (σ_Y equal to 0.5 and 1) [*Gelhar and Axness*, 1983] and against previously computed values for high heterogeneity (σ_Y equal to 3) [*de Dreuzy et al.*, 2007]. For σ_Y equal to 0.5 and 1, we find longitudinal dispersion coefficient values of 0.25 and 1.01, which are within less than 1% to the predicted values of 0.25 and 1. For σ_Y equal to 3, we find that the dispersion coefficient stabilizes at 19.5, within 2% of the previously obtained value of 19.1. The transverse dispersion coefficient is much smaller and can be identified only for σ_Y equal to 3. For σ_Y equal to 3, we find a value of 0.15 close to the value of 0.16 obtained by *de Dreuzy et al.* [2007].

[38] Second, we check that the temporal fluctuations of the mean velocity are consistently translated into the first moment of the particle positions. From equation (5), the time-dependent mean velocity has two nonzero components $\bar{u}_1 = [1 + \nu_1(t)]\bar{u}$ and $\bar{u}_2 = \nu_2(t)\bar{u}$. We check that these input values are closely matched by the mean particle velocities in both directions (Figure 2).

[39] We have thus checked that our methodology to compute the effective dispersion is consistent with the
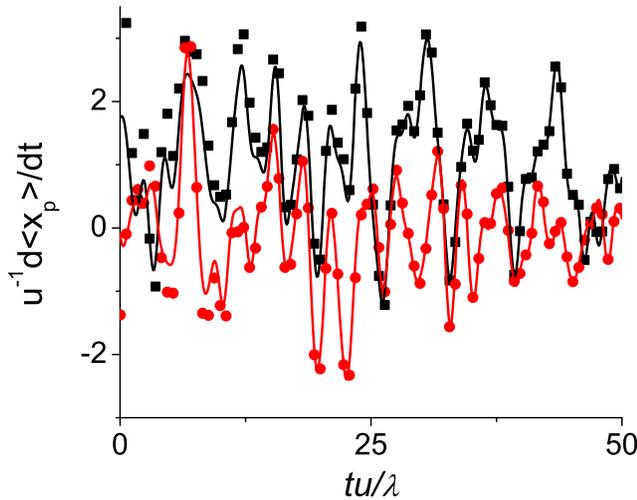
Figure 2. Comparison of the longitudinal and transverse mean particle velocities $d\langle x_p \rangle/dt$ normalized by the mean velocity $\bar{u}$ (squares and disks) with the imposed fluctuations (black and red lines) for one simulation taken with $\sigma_Y = 1$, $\sigma_{v1} = \sigma_{v2} = 1$ and $\rho = 0.5$.

existing results without temporal fluctuations and that the temporal fluctuations are correctly modeled.

3. Results

[40] We first present the results for configurations corresponding to uncorrelated ($\rho = 0$) and equally variable longitudinal and transverse fluctuations ($\sigma_{v1} = \sigma_{v2}$) and a Peclet number of 1000. We investigate the dependence of the asymptotic dispersion coefficients with the amplitude of the fluctuations. We then use these results as a reference for analyzing the effect of a correlation between longitudinal and transverse fluctuations and separate longitudinal or transverse fluctuations.

3.1. Equal Fluctuations in the Longitudinal and Transverse Directions

[41] Figure 3 display effective dispersion coefficients as functions of time for standard deviations of the log-permeability distribution σ_Y equal to 1 and 3, respectively. Both figures share common trends. Temporal fluctuations induce a decrease of the longitudinal effective dispersion (Figure 3a and Figure 4a) and an increase of the transverse effective dispersion (Figure 3b and Figure 4b). The longitudinal as well as the transverse effective dispersion coefficients display increasing variability when increasing the fluctuation amplitudes. This variability classically observed in the steady state case [*Bellin et al.*, 1992; *de Dreuzy et al.*, 2007; *Trefry et al.*, 2003] is enhanced by the temporal fluctuations. However, it does not prevent convergence of the effective dispersion toward an asymptotic value at late times. The insert of Figure 3b compares the temporal evolution of the effective second centered moment given by equation (14) for the highest-fluctuating case $\sigma_{v1} = \sigma_{v2} = 1$ (dots) to the trend that would be derived from the asymptotic transverse dispersion coefficient D_{2A} as computed with equations (16) and (17). The good agreement between
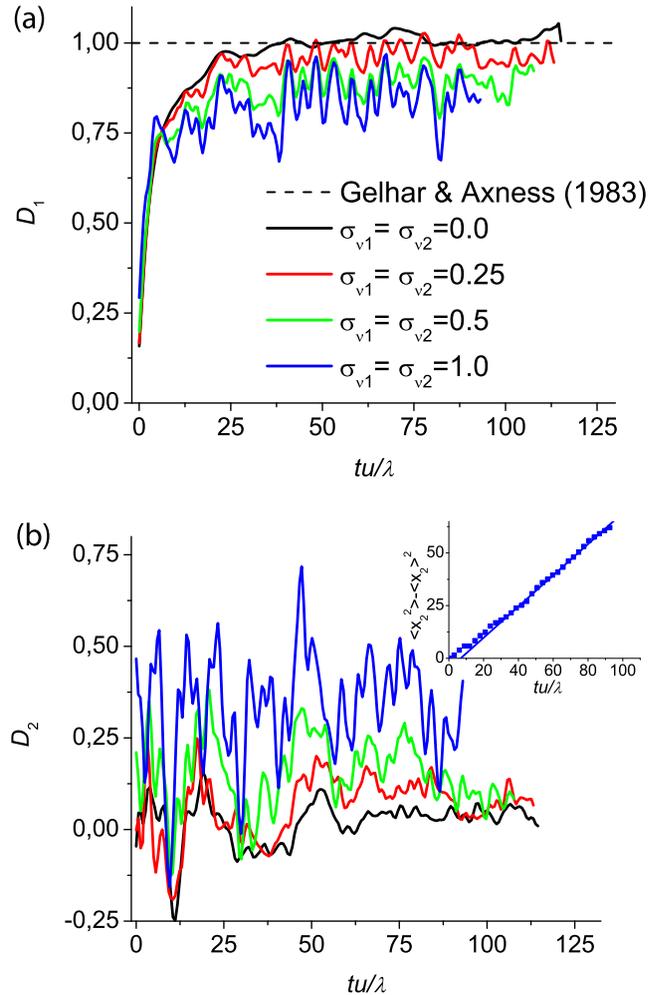

Figure 3. (a) Longitudinal D_1 and (b) transverse D_2 effective dispersion coefficients for $\sigma_Y^2 = 1$ without any correlation between longitudinal and transverse fluctuations ($\rho = 0$). The insert of Figure 3(b) shows the transverse variance of particle positions (dots) and the trend given by the asymptotic dispersion coefficient D_{2A} (line).

the variance of the particle transverse positions and the linear trend strengthens the reliability of the estimated transverse asymptotic dispersion coefficients.

[42] Figure 5 summarizes the asymptotic dispersion coefficients obtained from equations (16) and (17). For the small and moderate heterogeneity cases $\sigma_Y = 0.5$ and 1 (crosses and squares of Figure 5), transverse dispersion is critically enhanced by fluctuations as also shown by *Cirpka and Attinger* [2003]. Temporal fluctuations cause the steady state transverse dispersion coefficient to be multiplied by factors of 10 and 20 for $\sigma_{v1} = \sigma_{v2}$ equal to 0.5 and 1, respectively. As opposed to the transverse component, the longitudinal asymptotic dispersion is reduced by heterogeneity by at most 20% (Figure 5a). (see Figure 6.) Figure 7, obtained by injecting particles over only 2λ illustrates the strong increase of the transverse dispersion triggered by the simultaneous presence of temporal fluctuations and heterogeneity ($\sigma_{v1} = \sigma_{v2} = 1$).

[43] For the larger heterogeneity case $\sigma_Y = 3$, fluctuations also reduce the longitudinal asymptotic dispersion but
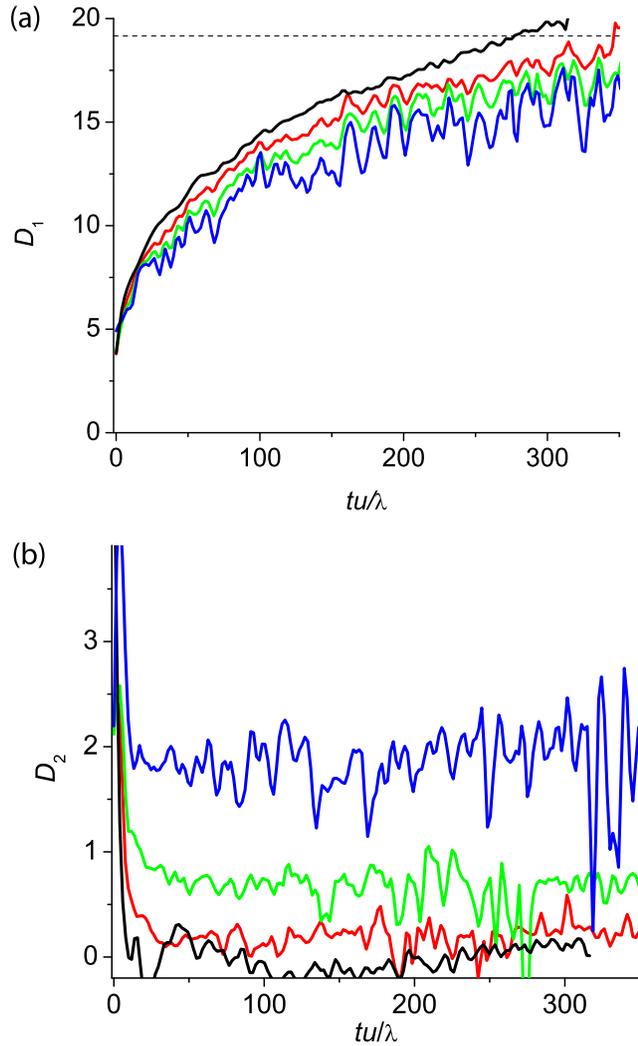
Figure 4. Same as Figure 3 for $\sigma_Y^2 = 9$.

Figure 5. (a) Longitudinal and (b) transverse asymptotic dispersion coefficients as functions of σ_{v1} and σ_{v2}. The longitudinal asymptotic dispersion coefficient D_{1A} is normalized by its value obtained without fluctuations.

almost in the same proportion as for the smaller heterogeneity case, $\sigma_Y^2 = 1$, as shown by the superposition of squares and stars on Figure 5a. In this large heterogeneity case, the effect of fluctuations is similar to that of diffusion in that both reduce the longitudinal asymptotic dispersion. For a Peclet number of 10^3, diffusion reduces the asymptotic dispersion by around 15% [de Dreuzy et al., 2007] while fluctuations reduce it by 10% to 20% for $\sigma_{v1} = \sigma_{v2}$ ranging from 0.5 to 1. The reduction induced by diffusion or fluctuations are comparable in this case. In the transverse direction, fluctuations still yield most of the enhancement of the transverse dispersion coefficient. Figure 8 illustrates even more than Figure 7 the simultaneous enhancement of the transverse dispersion and reduction of the longitudinal dispersion. For this particular realization, fluctuations cause the plume to be even more spread in the transverse than in the longitudinal direction.

[44] The effects of fluctuations on the absolute values of longitudinal and transverse macrodispersion are comparable whatever the heterogeneity level. Entering in details, however, we note the following difference. The total (sum of the longitudinal and transverse) dispersion increases with increasing fluctuations in the low-heterogeneity case,
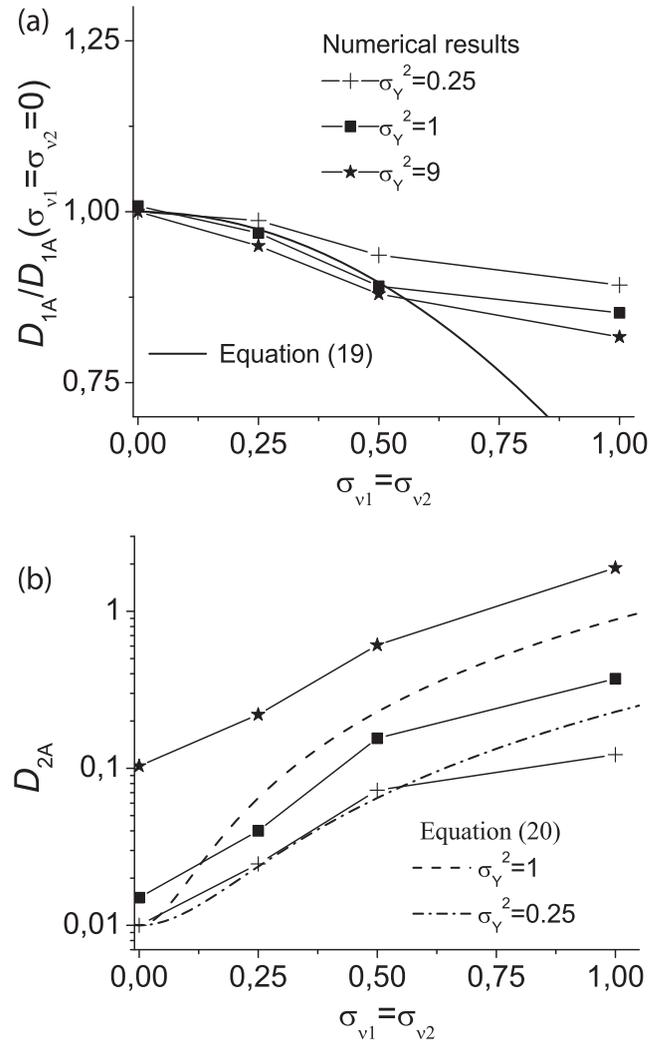
but decreases in the high-heterogeneity case (Figure 6). The sum increases by at most 30% and decreases by at most 10%. In the intermediate case $\sigma_Y = 1$, the sum remains almost constant for moderate variances of the temporal fluctuations ($\sigma_{v1} = \sigma_{v2} < 1$). This implies, first, that total dispersion is not strictly conserved when introducing fluctuations but also that it is not too far from conservative. Second, the enhancement of the transverse macrodispersion is larger than the reduction of the longitudinal macrodispersion for low heterogeneity. But the opposite occurs for high heterogeneity.

[45] We compare our numerical results with analytical approximations. These can be obtained from the results presented by Dentz et al. [2011] using a first-order perturbation expansion in σ_Y^2, σ_{v1}^2 and σ_{v2}^2 for flow and transport, which leads to

$$D_{1A}(\sigma_{\nu_1} = \sigma_{\nu_2}) = D_{1A}(\sigma_{\nu_1} = \sigma_{\nu_2} = 0)\left[1 - \sigma_{\nu_2}^2\left(\kappa^2 - \frac{\kappa + \kappa^3}{\sqrt{1+\kappa^2}}\right)\right]$$
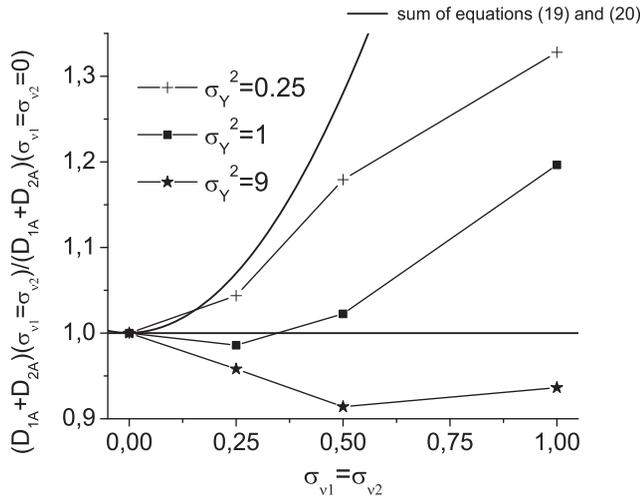
(19)

Figure 6. Sum of the longitudinal and transverse dispersions normalized by their steady state counterpart.

$$\frac{D_{2A}(\sigma_{\nu_1} = \sigma_{\nu_2})}{\lambda \bar{u}} = \sqrt{\frac{\pi}{2}} \sigma_Y^2 \sigma_{\nu_2}^2 \frac{\kappa}{\sqrt{1+\kappa^2}}, \qquad (20)$$

where we recall that κ is the Kubo number defined by equation (18). Analytical expressions and numerical results are qualitatively consistent (Figure 5). The agreement is excellent for the transverse asymptotic macrodispersion as long as σ_Y and σ_ν remain much smaller than 1 (Figure 5b, crosses versus dash-dotted line). The agreement is not as good for the longitudinal macrodispersion under the same conditions. For σ_Y and σ_ν approaching and larger than 1, numerical and analytical results differ significantly. Note that the analytical results of *Dentz and Carrera* [2005] differ from our numerical results. This is due to an inconsistency in the perturbation expansion for the effective dispersion coefficients, which is what motivated the work of *Dentz et al.* [2011].

3.2. Influence of Correlation Between Longitudinal and Transverse Fluctuations

[46] Table 1 compares the asymptotic dispersion coefficients computed with a partial correlation between the longitudinal and transverse fluctuations ($\rho = 0.5$) and without any correlation ($\rho = 0$). Differences are small. For $\sigma_{\nu 1} = \sigma_{\nu 2}$ equal to 0.5 and 1, the global trend of the correlation is to enhance the dispersion coefficients by at most 10% except for the transverse dispersion case with $\sigma_{\nu 1} = \sigma_{\nu 2} = 0.5$ and $\sigma_Y = 3$. In this case, the relevance of the value of 0.7 remains however limited because the transverse asymptotic value is almost not discernable behind the large temporal variability of the dispersion.

3.3. Separate Effects of Longitudinal and Transverse Fluctuations

[47] Table 2 displays the ratios of the dispersion coefficients computed with only longitudinal fluctuations (without any transverse fluctuations) to those without any fluctuations. For the longitudinal component, the ratios are equal to 0.98 or 0.99, which suggests that the longitudinal fluctuations do not have any influence on the longitudinal asymptotic dispersion coefficient. For the transverse component,

the ratios are slightly more variable between 0.95 and 1.17. Still, the transverse asymptotic dispersion coefficients remain very low, i.e., of the order or lower than the transverse asymptotic dispersion coefficient without fluctuations. They remain far below the order of magnitude enhancement of transverse dispersion obtained with both longitudinal and transverse fluctuations. In summary, longitudinal fluctuations hardly affect the asymptotic dispersion coefficients.

[48] To analyze the effect of the sole transverse fluctuations, we study a different ratio. Table 3 displays the ratio of the asymptotic dispersion coefficients obtained for the sole transverse fluctuations and for both longitudinal and transverse fluctuations. Both for the longitudinal and transverse components, the ratios are very close to 1, more precisely between 0.89 and 1.12. This shows that the effect of sole transverse fluctuations is comparable to that of both longitudinal and transverse fluctuations. The sole transverse fluctuations induce both the reduction of longitudinal dispersion and the enhancement of transverse dispersion.

[49] The effects of the longitudinal and transverse fluctuations cannot be rigorously summed because concentration depends nonlinearly on the velocity **u** in the advection diffusion equation (7). However, the previous results show empirically that the cumulative effects of the longitudinal and transverse fluctuations are in fact the sum of the effects of the sole longitudinal and transverse fluctuations. Everything happens as if the effect of both longitudinal and transverse fluctuations amounts to the sole effect of the transverse fluctuations irrespectively of longitudinal fluctuations. The weak influence of the correlation between longitudinal and transverse fluctuations reported in section 3.2 probably reflects the small influence of the longitudinal fluctuations. We underline that these results are so far demonstrated only for the asymptotic dispersion.

4. Discussion

[50] The most striking result concerns the behavior of the sum of the longitudinal and transverse dispersion coefficients, which we have termed total dispersion and which is not far from conservative, especially at moderate to high levels of heterogeneity ($\sigma_Y^2 > 1$). Strict conservation of the total dispersion had been obtained for sinusoidal fluctuations by *Goode and Konikow* [1990] but they assumed a homogeneous medium. In the analytical development of *Dentz et al.* [2011] the enhancement of transverse dispersion is also associated to a reduction of longitudinal dispersion for low levels of heterogeneity. However, the sum of both remains positive (dashed line of Figure 6) and larger than those derived from the numerical results. The deviation is largest for the high-heterogeneity case, when the reduction of longitudinal dispersion more than offsets the enhancement of transverse dispersion.

[51] These results are different from those published in the scientific literature. *Zhang and Neuman* [2003] predicted a decrease of longitudinal dispersion in response to transverse fluctuations, but also that it may decrease or increase in response to longitudinal fluctuations. *Rehfeldt and Gelhar* [2003] predicted that longitudinal decrease in response to transverse fluctuations. *Cirpka and Attinger* [2003] found an enhancement of the transverse dispersion without any variation of the longitudinal dispersion under
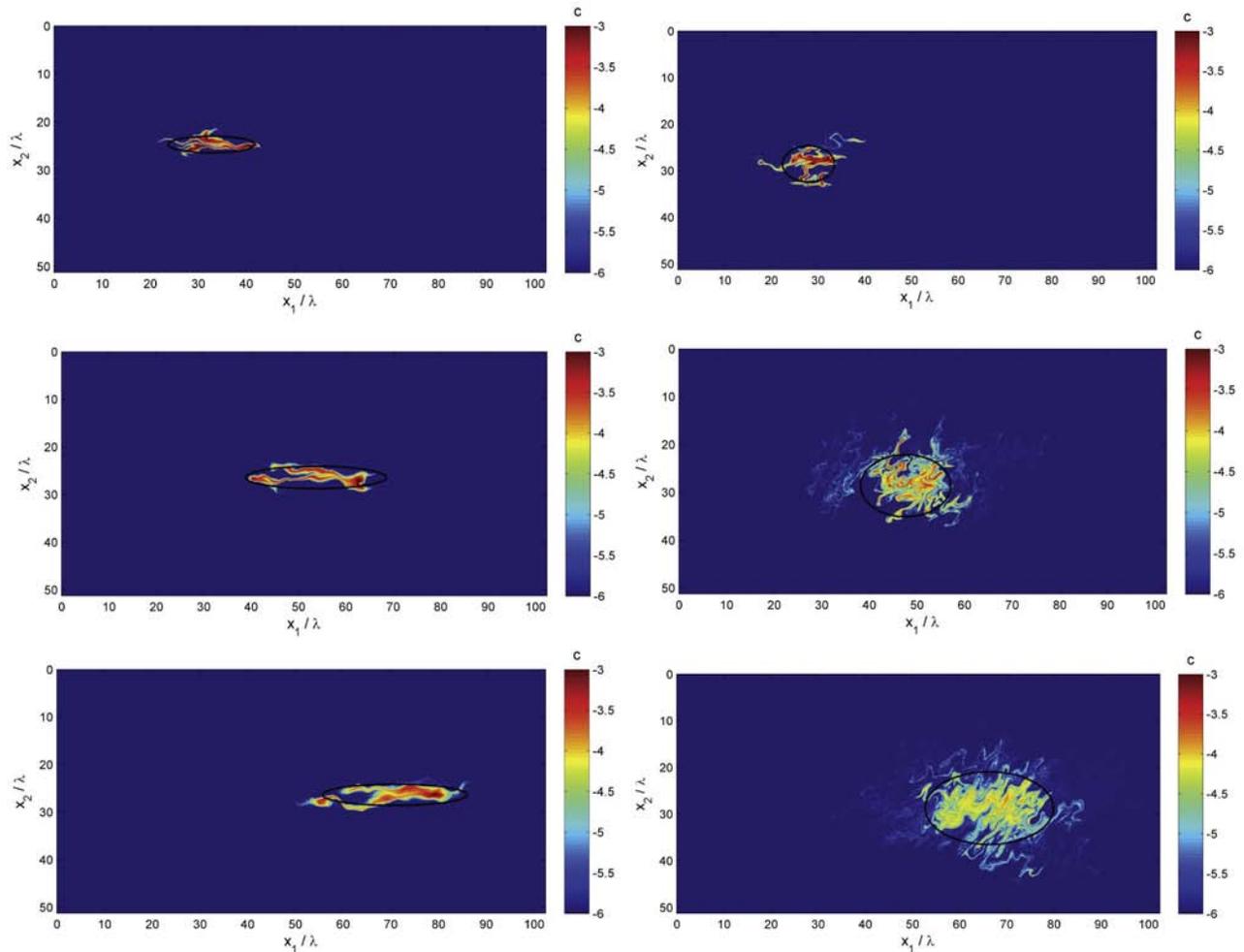
Figure 7. Evolution of the decimal logarithm of concentrations at three evolving times $t\bar{u}/\lambda =$ (top) 18, (middle) 36, and (bottom) 54 for the moderately heterogeneous case ($\sigma_Y = 1$). Simulations performed without fluctuations and with independent fluctuations in both the (right) longitudinal and (left) transverse directions, respectively, with the largest studied amplitudes $\sigma_{v1} = \sigma_{v2} = 1$. Five 10^5 particles have been injected 10λ downstream the left boundary condition along a vertical line of length 2λ. These injection conditions are different from the extended line source used for computing the asymptotic dispersion coefficients but better illustrate the dispersion tendencies. The black ellipse marks delimit twice the extension of the plume as computed by its standard deviations.

the assumption of sinusoidal transverse fluctuations. The longitudinal dispersion was obtained numerically on periodic unit cells with a random-walk method for transport. The origins of the difference may come non exclusively from the differences on the fluctuation type, on the Euclidean dimensionality (2-D here, 3-D in the work of *Cirpka and Attinger* [2003]) or from the limitations of unit cell simulations.

[52] The effect of fluctuations on dispersion can be addressed in the Lagrangian framework, where dispersion is equal to the time integral of the Lagrangian velocity correlation function [*Gelhar*, 1993]. In other words, the asymptotic dispersion coefficient is equal to the Lagrangian velocity variance times the integral correlation time scale. Temporal fluctuations broaden the Lagrangian velocity distribution in both the longitudinal and transverse directions (Figure 9). In the longitudinal direction (Figure 9a), the distribution of the absolute value of the first velocity

component $p(|u_1|)$ is broadened for both $\sigma_Y = 1$ and 3 both toward higher positive velocities and toward negative countercurrent velocities. In the transverse direction (Figure 9b), the distribution of the absolute value of the second velocity component $p(|u_2|)$ is extended toward higher values and as $p(u_2)$ is symmetrical around 0, the full distribution $p(u_2)$ is broadened toward both extremely low and high values. More quantitatively, from the steady state case to the highest temporal fluctuating case ($\sigma_{v1} = \sigma_{v2} = 1$), the variance of the Lagrangian velocity distribution increases by a factor 4 in the longitudinal direction and by 4 to 10 in the transverse direction.

[53] In the transverse direction for $\sigma_Y = 3$ and $\sigma_{v1} = \sigma_{v2} = 1$, the increase of the Lagrangian velocity variance by a factor of 10 causes the largest part of the dispersion enhancement of 15. By deduction, the remaining part of the enhancement comes from stronger correlations of the transverse component of the Lagrangian velocity. In the
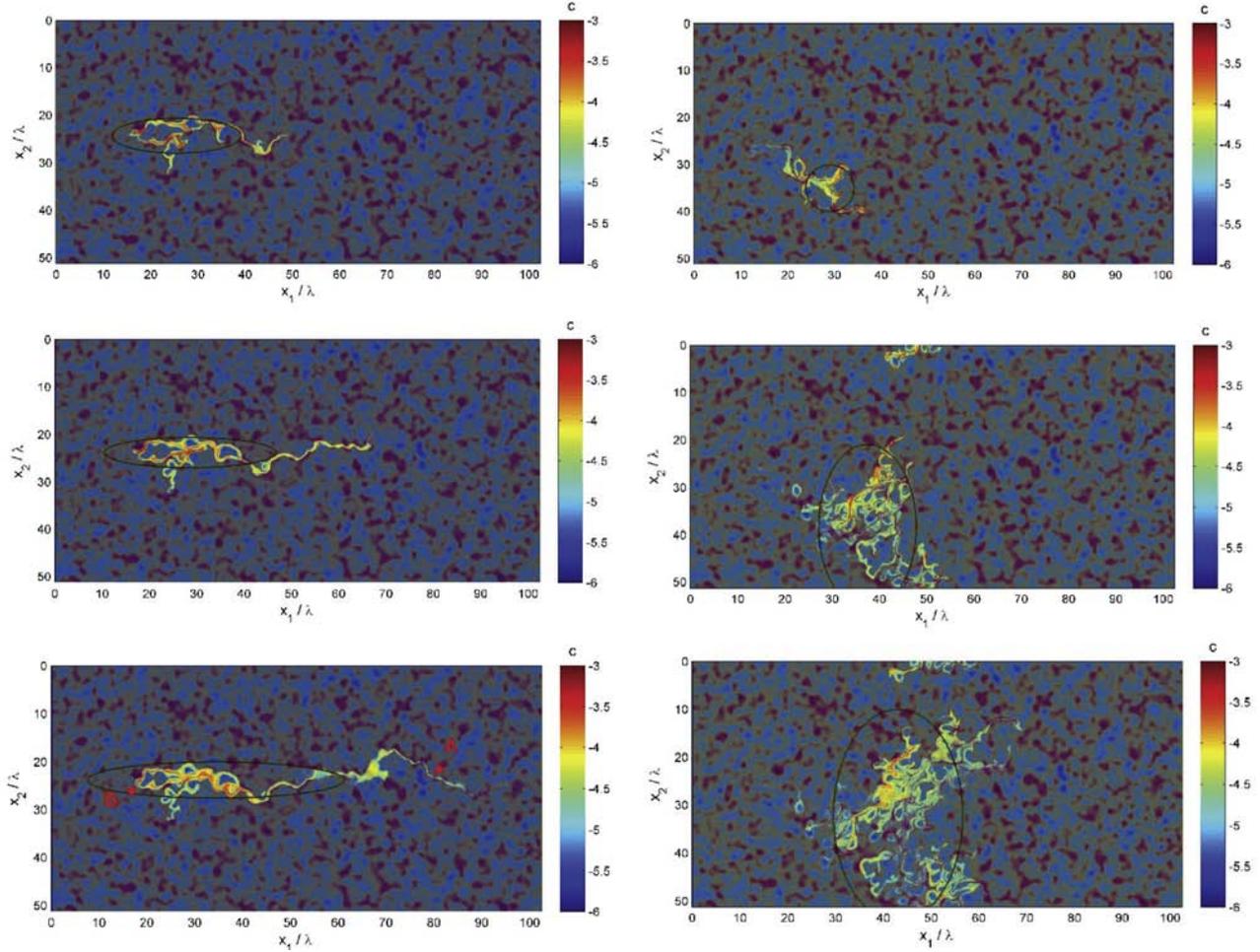
Figure 8. Same as Figure 7 for the highly heterogeneous case ($\sigma_Y = 3$) at three different times $t\bar{u}/\lambda =$ (top) 12, (middle) 18, and (bottom) 25. The permeability field has been superimposed in the background with permeability values increasing sharply from blue to red. Note on the right column the effect of the periodic boundary conditions that transfer virtually solute from the lower to the higher side of the system. However, for the computation of the transverse dispersion, everything happens as if particles are below or above the displayed domains. The real position of the solute (out of the system size) is however taken for the computation of the various plume moments.

longitudinal direction, dispersion decreases despite the four times increase of the variance of the longitudinal component of the Lagrangian velocity. By deduction, this indicates that the Lagrangian velocity correlation is reduced by a factor larger than 4 in the longitudinal direction. Temporal fluctuations thus enhance weakly the Lagrangian velocity correlation in the transverse direction but reduce it strongly in the longitudinal direction.

[54] These modifications of correlations are illustrated on the snapshots of the highly heterogeneous case (Figure 8). Without fluctuations, the plume stretches in the longitudinal direction. The fastest part of the solute ahead indicated by the red arrow marked A highlights a strongly correlated path of high longitudinal velocities. At the other end, the slowest part of the solute indicated by the red arrow marked B is held behind a small permeability zone.

Table 1. Ratio of Asymptotic Dispersion Coefficients With and Without Correlation Between the Longitudinal and Transverse Fluctuations

	$\sigma_{v1} = \sigma_{v2}$	$\dfrac{D_{1A}(\rho = 0.5)}{D_{1A}(\rho = 0)}$	$\dfrac{D_{2A}(\rho = 0.5)}{D_{2A}(\rho = 0)}$
$\sigma_Y^2 = 1$	0.5	1.00	1.00
$\sigma_Y^2 = 1$	1	0.99	1.06
$\sigma_Y^2 = 9$	0.5	1.04	0.70
$\sigma_Y^2 = 9$	1	1.03	1.10

Table 2. Ratio of Asymptotic Dispersion Coefficients With the Sole Longitudinal Fluctuations and Without Any Fluctuations

	σ_{v1}	$\dfrac{D_{1A}(\sigma_{v1}, \sigma_{v2} = 0)}{D_{1A}(\sigma_{v1} = 0, \sigma_{v2} = 0)}$	$\dfrac{D_{2A}(\sigma_{v1}, \sigma_{v2} = 0)}{D_{2A}(\sigma_{v1} = 0, \sigma_{v2} = 0)}$
$\sigma_Y^2 = 1$	0.5	0.99	1.17
$\sigma_Y^2 = 1$	1.0	0.99	1.15
$\sigma_Y^2 = 9$	0.5	0.98	0.95
$\sigma_Y^2 = 9$	1.0	0.99	0.92

Table 3. Ratio of Asymptotic Dispersion Coefficients With the Sole Transverse Fluctuations and With Both Fluctuations

	σ_{v2}	$\dfrac{D_{1A}(\sigma_{v1}=0,\sigma_{v2})}{D_{1A}(\sigma_{v1}=\sigma_{v2})}$	$\dfrac{D_{2A}(\sigma_{v1}=0,\sigma_{v2})}{D_{2A}(\sigma_{v1}=\sigma_{v2})}$
$\sigma_Y^2=1$	0.5	1.00	1.06
$\sigma_Y^2=1$	1.0	0.89	1.02
$\sigma_Y^2=9$	0.5	1.00	1.04
$\sigma_Y^2=9$	1.0	1.03	1.12

The solute is blocked by slow advection behind a low permeability zone that acts as a barrier. To a lesser extent, it is also trapped by diffusion within the low-K zone. The solute gets away from blocking barriers and from diffusion traps by slowly flowing around them.

[55] Transverse fluctuations affect both ends of the plume. On the one hand, they carry solute away from the high-velocity paths in the leading edge of the plume. As a result, the mean velocity of the leading portion of the

Figure 9. Asymptotic distribution of the (a) longitudinal and (b) transverse components of the absolute value of the velocity sampled by the particles with independent fluctuations ($\sigma_{v1} = \sigma_{v2} = 1$) and without fluctuations (steady state) for moderately ($\sigma_Y = 1$) and highly ($\sigma_Y = 3$) heterogeneous cases.

plume is reduced. Effectively, as argued by *Zhang and Neuman* [1996] for the conditional Eulerian velocity covariance, the correlation of the leading particles is reduced at the plume front by transverse fluctuations in the head gradient.

[56] The trailing end of the plume, on the other hand is accelerated by transverse fluctuations because they facilitate the solute getting away from flow barriers. They also affect trapping, but to a lesser extent (compare diffusion rings with and without fluctuations in Figure 7). In fact a few trapping rings can be observed trailing the plume in Figure 6. However, by reducing blocking time, transverse fluctuations also reduce the relative importance of trapping. Again, the Langragian correlation time is reduced. Notice, however, that these effects would hardly be noticeable in terms of Eulerian covariances because the velocity is small, so that correlation is restricted to short distances.

[57] The effect of the reduction of the longitudinal dispersion is analogous to that obtained under steady state conditions with diffusion as conjectured in the introduction [*de Dreuzy et al.*, 2007]. The origins of the effects are however different. Diffusion has a double effect of reducing the velocity variance and the Lagrangian velocity correlation. Both of these effects lead to a reduction of the kinematic dispersion. In the case of temporal fluctuations, the effect of the reduction of the Lagrangian correlation dominates that of the increase of the velocity variability (Figure 9). Reduction of correlation is the most important mechanism and yields a similar effect as in Taylor dispersion [*Taylor*, 1953]. In fact, the Taylor dispersion coefficient is inversely proportional to the diffusion coefficient that induces the reduction of correlation of the Lagrangian velocity.
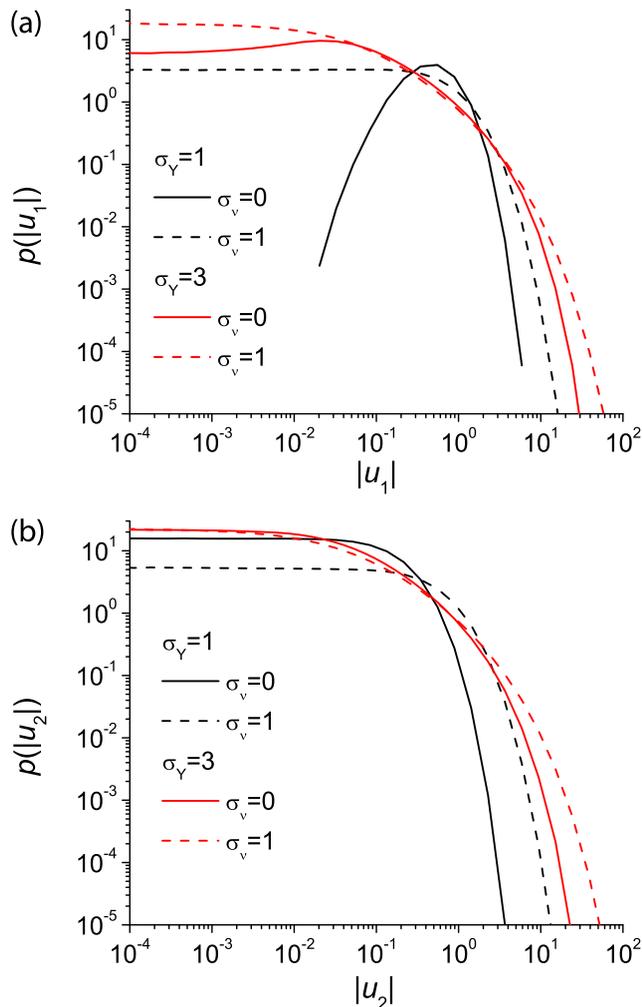
5. Conclusions

[58] We have studied the cumulative effects of heterogeneity and temporal fluctuations of the flow conditions on the asymptotic dispersion coefficients. The longitudinal and transverse dispersion coefficients have been estimated by using extensive Monte Carlo simulations on large domains.

[59] Numerical results show that fluctuations parallel to the main flow directions hardly change the macrodispersion coefficients. As longitudinal fluctuations do not alter the flow lines, they have a limited impact on macrodispersion. This implies that the decomposition of the fluctuations in longitudinal and transverse components is more relevant than the other possible decomposition in direction and amplitude as the sole influential fluctuation is the transverse one. It also implies that this conclusion will hold in 3-D systems.

[60] Transverse temporal fluctuations (1) enhance transverse spreading and (2) reduce longitudinal spreading. Enhancement of transverse spreading comes from the widening of the velocity distribution supplemented by the increase of the correlation of the transverse Lagrangian velocity. Reduction of longitudinal spreading comes from the deceleration of the plume front and acceleration of the plume tail that dominates the widening of the velocity distribution. As a result of these opposed trends on the longitudinal and transverse dispersions, the total dispersion (sum of the longitudinal and transverse dispersion coefficients) is not far from conservative. That is, temporal fluctuations cause little change in total dispersion with respect to the

value obtained for steady state flux. Still, for high heterogeneity, this change occurs in the direction of somewhat reducing total dispersion in response to temporal fluctuations which contradicts expectations.

[61] Direct perspectives of this work are the analyses of the apparent influence of temporal fluctuations on the duration of the preasymptotic regime and on mixing. As shown by Figure 4, temporal fluctuations let transverse dispersion converge at once to its asymptotic value while, in the longitudinal direction, the convergence rate remains almost unchanged. We also intend to quantify the strong mixing effect hinted by Figure 7 and Figure 8 with the new methods developed recently for the steady state case [*Le Borgne et al.*, 2010, 2011]. Although desirable, the extension of these results to 3-D systems is currently hindered by high computational costs.

References

Ababou, R., et al. (1989), Numerical simulation of three-dimensional saturated flow in randomly heterogeneous porous media, *Transp. Porous Media*, *4*(6), 549–565.

Ackerer, P., and W. Kinzelbach (1985), Modélisation du transport de contaminant par la méthode de marche au hasard: Influence des variations du champ d'écoulement au cours du temps sur la dispersion, paper presented at Approach to Subsurface Flow, Int. Assoc. Hydraul. Res., Montvillargene, France.

Alabert, F. (1987), The practice of fast conditional simulations through the LU decomposition of the covariance matrix, *Math. Geol.*, *19*(5), 369–386.

Beaudoin, A., et al. (2007), An efficient parallel tracker for advection-diffusion simulations in heterogeneous porous media, in *Europar*, vol. 4641, pp. 705–714, Springer, New York.

Beaudoin, A., J.-R. de Dreuzy, and J. Erhel (2010), Numerical Monte Carlo analysis of the influence of pore-scale dispersion on macrodispersion in 2-D heterogeneous porous media, *Water Resour. Res.*, *46*, W12537, doi:10.1029/2010WR009576.

Bellin, A., P. Salandin, and A. Rinaldo (1992), Simulation of dispersion in heterogeneous porous formations: Statistics, first-order theories, convergence of computations, *Water Resour. Res.*, *28*(9), 2211–2227, doi:10.1029/92WR00578.

Chavent, G., and J. E. Roberts (1991), A unified physical presentation of mixed, mixed-hybrid finite elements and standard finite difference approximations for the determination of velocities in waterflow problems, *Adv. Water Resour.*, *14*(6), 329–348.

Cirpka, O. A., and S. Attinger (2003), Effective dispersion in heterogeneous media under random transient flow conditions, *Water Resour. Res.*, *39*(9), 1257, doi:10.1029/2002WR001931.

Dagan, G. (1984), Solute transport in heterogeneous porous formations, *J. Fluid. Mech.*, *145*, 151–177.

Dagan, G. (1989), *Flow and Transport in Porous Formations*, 465 pp., Springer, New York.

Dagan, G., A. Bellin, and Y. Rubin (1996), Lagrangian analysis of transport in heterogeneous formations under transient flow conditions, *Water Resour. Res.*, *32*(4), 891–899, doi:10.1029/95WR02497.

Davis, M. W. (1987), Production of conditional simulations via the LU triangular decomposition of the covariance matrix, *Math. Geol.*, *19*(2), 91–98.

de Dreuzy, J.-R., A. Beaudoin, and J. Erhel (2007), Asymptotic dispersion in 2D heterogeneous porous media determined by parallel numerical simulations, *Water Resour. Res.*, *43*, W10439, doi:10.1029/2006WR005394.

Delay, F., et al. (2005), Solution of solute transport in porous or fractured formations by random walk particle tracking: A review, *Vadose Zone J.*, *4*, 360–379.

Dentz, M., and J. Carrera (2003), Effective dispersion in temporally fluctuating flow through a heterogeneous medium, *Phys. Rev. E*, *68*(3), 036310, doi:10.1103/PhysRevE.68.036310.

Dentz, M., and J. Carrera (2005), Effective solute transport in temporally fluctuating flow through heterogeneous media, *Water Resour. Res.*, *41*, W08414, doi:10.1029/2004WR003571.

Dentz, M., H. Kinzelbach, S. Attinger, and W. Kinzelbach (2000), Temporal behavior of a solute cloud in a heterogeneous porous medium, 1, Point-like injection, *Water Resour. Res.*, *36*(12), 3591–3604, doi:10.1029/2000WR900162.

Dentz, M., et al. (2011), Erratum: Effective dispersion in temporally fluctuating flow through a heterogeneous medium, *Phys. Rev. E*, *84*, 019904, doi:10.1103/PhysRevE.84.019904.

Englert, A., J. Vanderborght, and H. Vereecken (2006), Prediction of velocity statistics in three-dimensional multi-Gaussian hydraulic conductivity fields, *Water Resour. Res.*, *42*, W03418, doi:10.1029/2005WR004014.

Erhel, J., et al. (2009), A parallel scientific software for heterogeneous hydrogeoloy, in *Parallel Computational Fluid Dynamics 2007*, vol. 67, pp. 39–48, Springer, New York.

Falgout, R. D., et al. (2005), Pursuing scalability for HYPRE's conceptual interfaces, *ACM Trans. Math. Software*, *31*(3), 326–350.

Festger, A. D., and G. R. Walter (2002), The capture efficiency map: The capture zone under time-varying flow, *Ground Water*, *40*(6), 619–628.

Frigo, M., and S. G. Johnson (2005), The design and implementation of FFTW3, *Proc. IEEE*, *93*, 216–231.

Gelhar, L. W. (1993), *Stochastic Subsurface Hydrology*, Prentice Hall, Engelwood Cliffs, N. J.

Gelhar, L. W., and C. L. Axness (1983), Three-dimensional stochastic analysis of macrodispersion in aquifers, *Water Resour. Res.*, *19*, 161–180.

Gelhar, L. W., C. Welty, and K. R. Rehfeldt (1992), A critical review of data on field-scale dispersion in aquifers, *Water Resour. Res.*, *28*(7), 1955–1974, doi:10.1029/92WR00607.

Goode, D. J., and L. F. Konikow (1990), Apparent dispersion in transient groundwater flow, *Water Resour. Res.*, *26*(10), 2339–2351.

Gutjahr, A. L. (1989), Fast Fourier transforms for random field generation, *N. M. Tech. Proj. Rep. 4-R58-2690R*, New Mexico Inst. of Mining and Tech., Socorro, NM.

Kinzelbach, W. (1988), The random-walk method in pollutant transport simulation, in Groundwater Flow and Quality Modelling, NATO ASI Ser. C, vol. C224, pp. 227–246, Springer, New York.

Kinzelbach, W., and P. Ackerer (1986), Modélisation de la propagation d'un contaminant dans un champ d'écoulement transitoire, *Hydrogéologie*, *2*, 197–206.

Kitanidis, P. K. (1988), Prediction by the method of moments of transport in a heterogeneous formation, *J. Hydrol.*, *102*(1–4), 453–473.

Le Borgne, T., et al. (2010), Non-Fickian mixing: Temporal evolution of the scalar dissipation rate in heterogeneous porous media, *Adv. Water Resour.*, *3*(12), 1468–1475.

Le Borgne, T., et al. (2011), Persistence of incomplete mixing: A key to anomalous transport, *Phys. Rev. E*, *84*(1), 015301, doi:10.1103/PhysRevE.84.015301.

Le Ravalec, M., et al. (2000), The FFT moving average (FFT-MA) generator: An efficient numerical method for generating and conditioning gaussian simulations, *Math. Geol.*, *32*(6), 701–723.

Matheron, G. (1967), *Eléments Pour une Théorie des milieux Poreux*, Masson, Paris.

Naff, R. L., T.-C. Yeh, and M. Kemblowski (1989), Reply, *Water Resour. Res.*, *25*(12), 2523–2525.

Neuman, S., C. L. Winter, and C. M. Newman (1987), Stochastic theory of field-scale fickian dispersion in anisotropic porous media, *Water Resour. Res.*, *23*(3), 453–466.

Pardo-Iguzquiza, E., and M. Chica-Olmo (1993), The Fourier integral method—An efficient spectral method for simulation of random fields, *Math. Geol.*, *25*(2), 177–217.

Pollock, D. W. (1988), Semianalytical computation of path lines for finite-difference models, *Ground Water*, *26*(6), 743–750.

Ramirez, J. M., E. A. Thomann, E. C. Waymire, J. Chastanet, and B. D. Wood (2008), A note on the theoretical foundations of particle tracking methods in heterogeneous porous media, *Water Resour. Res.*, *44*, W01501, doi:10.1029/2007WR005914.

Rehfeldt, K. R., and L. W. Gelhar (1992), Stochastic analysis of dispersion in unsteady flow in heterogeneous aquifers, *Water Resour. Res.*, *28*(8), 2085–2099.

Salamon, P., et al. (2006), A review and numerical assessment of the random walk particle tracking method, *J. Contam. Hydrol.*, *87*(3–4), 277–305.

Salandin, P., and V. Fiorotto (1998), Solute transport in highly heterogeneous aquifers, *Water Resour. Res.*, *34*(5), 949–961.

Sudicky, E. A. (1986), A natural gradient experiment on solute transport in a sand aquifer: Spatial variability of hydraulic conductivity and its role in the dispersion process, *Water Resour. Res.*, *22*(13), 2069–2082.

Sykes, J. F., S. B. Pahwa, R. B. Lantz, and D. S. Ward (1982), Numerical simulation of flow and contaminant migration at an extensively monitored landfill, *Water Resour. Res.*, *18*(6), 1687–1704.

Taylor, G. (1953), Dispersion of soluble matter in solvent flowing slowly through a tube, *Proc. R. Soc. London Ser. A*, *219*(1137), 186–203.

Trefry, M. G., F. P. Ruan, and D. McLaughlin (2003), Numerical simulations of preasymptotic transport in heterogeneous porous media: Departures from the Gaussian limit, *Water Resour. Res.*, *39*(3), 1063, doi:10.1029/2001WR001101.

van Kampen, N. G. (1981), *Stochastic Processes in Physics and Chemistry*, Elsevier, New York.

Wen, X. H., and J. J. Gomez-Hernandez (1996), The constant displacement scheme for tracking particles in heterogeneous aquifers, *Ground Water*, *34*(1), 135–142.

Zhang, D. X., and S. P. Neuman (1996), Head and velocity covariances under quasi-steady state flow and their effects on advective transport, *Water Resour. Res.*, *32*(1), 77–83.

J. Carrera, J.-R. de Dreuzy and M. Dentz, GHS, Institute of Environmental Analysis and Water Studies, C/ Jordi Girona 18–26, 08034 Barcelona, Spain. (jean-raynald.de-dreuzy@univ-rennes1.fr)

T. Le Borgne, Géosciences Rennes, UMR CNRS 6118, Université de Rennes 1, Campus de Beaulieu, 263 avenue du Général Leclerc, 35042 Rennes cedex, France.